Absolute Value Layered ACO-OFDM for Intensity-Modulated Optical Wireless Channels

Ruowen Bai, and Steve Hranilovic
Department of Electrical and Computer Engineering, McMaster University, ON., Canada
Email:{bair4, hranilovic}@mcmaster.ca

***Abstract*—Both enhanced unipolar orthogonal frequency division multiplexing (eU-OFDM) and layered asymmetrically clipped optical OFDM (LACO-OFDM) are among the most spectrally efficient modulation techniques for intensity modulated links that layer multiple non-negative signals. In this paper, we propose *absolute value layered asymmetrically clipped optical OFDM* (ALACO-OFDM) which further improves the spectral efficiency while using a smaller number of layers and no direct current (DC) bias. In ALACO-OFDM, asymmetrically clipped optical OFDM (ACO-OFDM) signals are sent at the first L layers and absolute value optical OFDM (AVO-OFDM) is used for the remaining subcarriers and transmitted simultaneously. Analysis indicates that ALACO-OFDM achieves higher spectral efficiency and smaller peak-to-average power ratio (PAPR) compared to eU-OFDM, LACO-OFDM and asymmetrically clipped absolute value optical OFDM (AAO-OFDM). Monte Carlo simulation results also indicate that ALACO-OFDM achieves significant bit error rate (BER) performance gains compared to its counterparts at the same spectral efficiency.**

***Index Terms*—Orthogonal frequency division multiplexing (OFDM), LACO-OFDM, eU-OFDM, AAO-OFDM, intensity modulation with direct detection (IM/DD).**

I. Introduction

While a majority of wireless communications systems operate in the radio bands, optical wireless communications (OWC) has recently emerged as an attractive complementary link due to the ubiquity of solid-state illumination and the availability of large amounts of unregulated spectrum [1], [2]. Data are conveyed by modulating the instantaneous optical intensity (i.e., intensity modulation (IM)) and detecting the received signal power using a photodiode (i.e., direct detection (DD)). Such IM/DD links impose constraints on the non-negativity of all emitted signals and constrain the average amplitude [1]–[3].

Many of these optical wireless channels, especially those that arise due to visible light communications (VLC), are bandwidth limited. In this context spectrally efficient orthogonal frequency division multiplexing (OFDM) has been investigated for OWC to enhance the data rate while satisfying IM/DD amplitude constraints. To generate a real-value time-domain signal, Hermitian symmetry in the spectrum is required [4]. However, many approaches exist to ensure amplitude non-negativity. In direct current (DC) biased optical OFDM (DCO-OFDM) a conventional OFDM signal is biased to ensure non-negativity. Although this preserves its high spectral efficiency, the addition of a large DC bias makes this approach power inefficient [4]. Approaches such as asymmetrically clipped optical OFDM (ACO-OFDM) [5] and unipolar OFDM (U-OFDM) [6] are more power efficient and ensure amplitude non-negativity at a cost of half of the spectral efficiency. To address this spectral efficiency loss, enhanced U-OFDM (eU-OFDM) [6], layered ACO-OFDM (LACO-OFDM) [7]–[10] and asymmetrically clipped absolute value optical OFDM (AAO-OFDM) [3] have been proposed in which no explicit DC bias is required. In general, these approaches work by layering a number of non-negative signals and performing successive detection at the receiver. In theory, the spectral efficiency of eU-OFDM and LACO-OFDM approach that of DCO-OFDM as the number of layers or streams increases. However, using a large number of layers incurs high computational complexity and latency in the demodulator. For AAO-OFDM, which has only two streams, the spectral efficiency is 0.5 bit/s/Hz smaller than DCO-OFDM.

In this paper, *absolute value layered ACO-OFDM* (ALACO-OFDM) is presented which has a high spectral efficiency approaching that of DCO-OFDM while preserving power efficiency. In ALACO-OFDM, ACO-OFDM signals are sent in the first L layers and absolute value optical OFDM (AVO-OFDM) [3] is used at the remaining subcarriers. These streams are superimposed in the time domain and transmitted simultaneously. No explicit DC bias is required. The sign information bits of AVO-OFDM are inserted uniformly into the first ACO-OFDM layer. At the receiver, the L layers of ACO-OFDM symbols are first demodulated layer-by-layer as in LACO-OFDM [8] and then the AVO-OFDM symbols are demodulated with the aid of sign information conveyed in the first layer. Analysis indicates that ALACO-OFDM with a given number of layers L achieves higher spectral efficiency than eU-OFDM, LACO-OFDM and AAO-OFDM. In addition, the peak-to-average power ratio (PAPR) of ALACO-OFDM is shown to be smaller than its counterparts suggesting it is less prone to clipping distortion. The bit error rate (BER) performance based on Monte Carlo simulations is also presented and ALACO-OFDM is shown to be more power efficient than eU-OFDM and LACO-OFDM when operating at the same spectral efficiency and error rate.

The balance of the paper is organized as follows. Section II defines the ALACO-OFDM transmitter and receiver. Spectral efficiency and PAPR performance of the ALACO-OFDM are analyzed and compared to its counterparts in Section III, and the BER performance is presented and compared in Section IV. Finally, conclusions are drawn in Section V.

978-1-5386-8088-9/19/$31.00 ©2019 IEEE

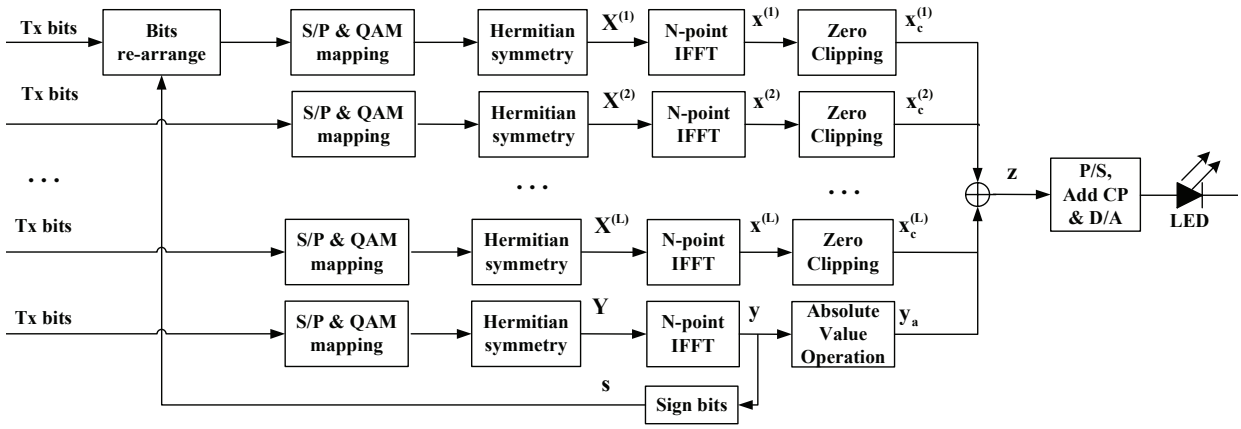

Fig. 1. Transmitter design block diagram for ALACO-OFDM.

II. Definition of ALACO-OFDM

A. Transmitter

The transmitter block diagram for an ALACO-OFDM based IM/DD system with N subcarriers is shown in Fig. 1, in which N is a power of 2. The ALACO-OFDM signal consists of L layers of ACO-OFDM [8] and a single layer of AVO-OFDM [3].

Transmitted bits are serial-to-parallel (S/P) converted and mapped to quadrature amplitude modulation (QAM) constellation symbols. To obtain a real-valued time-domain signal, Hermitian symmetry is imposed on the N subcarriers, where $X_k = X^*_{N-k}$, and X_0 and $X_{N/2}$ are set to zero [4].

For the first layer ACO-OFDM, the constellation symbols are mapped onto odd subcarriers, i.e., X_{2k+1} for $k = 0, 1, 2, \cdots, N/4-1$), in a frame and unused subcarriers are set to zero. After applying Hermitian symmetry, the frequency-domain symbol vector $\mathbf{X}^{(1)}$ is given by

$$\mathbf{X}^{(1)} = \left[0, X_1, 0, X_3, 0, \cdots, X_{N/2-1}, 0, X^*_{N/2-1}, \cdots, 0, X^*_1\right]. \tag{1}$$

For the second layer ACO-OFDM, constellation symbols are mapped onto $X_{2(2q+1)}$ for $q = 0, 1, 2, \cdots, N/8-1$ and remaining subcarriers are set to zero. The frequency-domain symbol vector $\mathbf{X}^{(2)}$ is

$$\mathbf{X}^{(2)} = [0, 0, X_2, 0, 0, 0, X_6, 0, \cdots, X^*_6, 0, 0, 0, X^*_2, 0]. \tag{2}$$

In general, for the l-th layer ACO-OFDM ($l = 1, \cdots, L$ and $L < \log_2 N - 1$), the constellation symbols are mapped onto $X_{2^{l-1}(2q+1)}$ for $q = 0, 1, 2, \cdots, P(l)-1$ where

$$P(l) = \frac{N}{2^{l+1}}$$

with all other subcarriers set to zero. The resulting frequency domain symbol vector $\mathbf{X}^{(l)}$ is

$$\mathbf{X}^{(l)} = [0, \cdots, 0, X_{2^{l-1}}, 0, \cdots, 0, X_{3\cdot 2^{l-1}}, 0, \cdots, 0, X^*_{2^{l-1}}, 0, \cdots, 0]. \tag{3}$$

Next, an N-point inverse fast Fourier transform (IFFT) is performed on $\mathbf{X}^{(l)}$ at l-th layer to obtain a bipolar time-domain signal vector $\mathbf{x}^{(l)}$, where the n-th element is defined as

$$x_n^{(l)} = \frac{1}{\sqrt{N}} \sum_{k=0}^{N-1} X_k{}^{(l)} \exp\left(j\frac{2\pi}{N}nk\right),\ 0 \le n \le N-1. \tag{4}$$

As shown in [8], $\mathbf{x}^{(l)}$ is a real-valued bipolar vector with a period of $4P(l) = \frac{N}{2^{l-1}}$, and has an anti-symmetry as

$$x_n^{(l)} = -x^{(l)}_{n+2P(l)},\ 0 \le n \le 2P(l)-1. \tag{5}$$

Therefore, the negative part of $\mathbf{x}^{(l)}$ can be directly clipped without losing any information leading to ACO-OFDM time-domain signal $\mathbf{x}_c^{(l)}$ at the l-th layer [8].

After L layers of ACO-OFDM, there remain $2P(L)$ subcarriers that are unused. Consider using AVO-OFDM [3] to send data on these unused carriers. Specifically, QAM symbols are mapped onto Y_{q2^L} for $q = 1, 2, \cdots, P(L)-1$ with other subcarriers set to zero. After Hermitian symmetry, the frequency-domain symbol vector $\mathbf{Y}$ is given as

$$\mathbf{Y} = [0, \cdots, 0, Y_{2^L}, 0, \cdots, 0, Y_{2\cdot 2^L}, 0, \cdots, 0, Y^*_{2^L}, 0, \cdots, 0]. \tag{6}$$

The time-domain signal y_n is obtained via the IFFT to give

$$y_n = \frac{1}{\sqrt{N}} \sum_{k=0}^{N-1} Y_k \exp\left(j\frac{2\pi}{N}nk\right),\ 0 \le n \le N-1. \tag{7}$$

Substituting (6) into (7) gives

$$y_n = \frac{1}{\sqrt{N}} \sum_{q=0}^{2P(L)-1} Y_{q2^L} \exp\left(j\frac{2\pi}{2P(L)}qn\right) \tag{8}$$

where $0 \le n \le N-1$. From (8), notice that $\mathbf{y}$ has a period of $2P(L)$, i.e.,

$$y_n = y_{n+2P(L)}. \tag{9}$$

To ensure non-negativity, define $y_{a,n}$ as

$$y_{a,n} = |y_n|,\ 0 \le n \le N-1 \tag{10}$$

where $|\cdot|$ denotes absolute value operation. Considering $\mathbf{y}$ has a

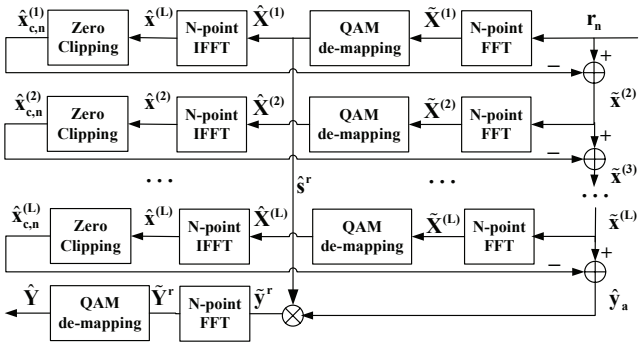

Fig. 2. Receiver design block diagram for ALACO-OFDM.

period of $2P(L)$, only $2P(L)$ sign bits need to be transmitted to reconstruct the original AVO-OFDM signal. Let the vector of sign bits be denoted as $\mathbf{s}$, with components [3]

$$s_n = \begin{cases} 0, & y_n \leq 0; \\ 1, & y_n > 0, \end{cases} \tag{11}$$

where $0 \leq n \leq 2P(L)-1$. These sign bits are inserted uniformly over transmitting symbols mapped to symbol vector $\mathbf{X}^{(1)}$, which is transmitted by the first layer ACO-OFDM.

Adding together the L layer ACO-OFDM signals $\mathbf{x}_c^{(l)}$ and AVO-OFDM signal $\mathbf{y}_a$, the discrete time-domain transmitted signal vector is denoted $\mathbf{z}$ with components

$$z_n = \sum_{l=1}^{L} x_{c,n}^{(l)} + y_{a,n},\ 0 \leq n \leq N-1. \tag{12}$$

Finally, after parallel-to-serial (P/S) conversion and the addition of a a cyclic prefix (CP) added, $\mathbf{z}$ is fed into a digital-to-analog (D/A) converter before driving an LED.

B. Receiver

At the receiver, a photo-diode (PD) is utilized to convert the received optical signal into an electrical current. The shot noise and thermal noise are modelled as additive white Gaussian noise (AWGN) [5], [8]. As this paper focuses on transceiver design, here we consider a flat channel with perfect equalization and synchronization and the channel gain from the LED to the PD is assumed to be unity [5], [6].

The receiver block diagram is depicted in Fig. 2. After S/P conversion, analog-to-digital (A/D) conversion and removal of the CP, the received signal r_n is

$$r_n = z_n + w_n,\ 0 \leq n \leq N-1 \tag{13}$$

where w_n denotes the discrete sample of AWGN.

The clipping distortion of l-th ($1 \leq l \leq L$) layer ACO-OFDM falls on subcarriers of higher layers; that is, the l-th layer ACO-OFDM should be demodulated before the $(l+1)$-th layer [8]. Notice also that from (9) and (10) that $\mathbf{y}_a$ has a period of $2P(L)$. Thus, its discrete Fourier transform (DFT) can be written as

$$\begin{aligned} Y_{a,k} &= \frac{1}{\sqrt{N}} \sum_{n=0}^{N-1} y_{a,n} \exp\left(-j\frac{2\pi}{N}nk\right) \\ &= \begin{cases} \frac{2^L}{\sqrt{N}} \sum_{n=0}^{2P(L)-1} y_{a,n} \exp\left(-j\frac{2\pi}{N}nk\right), & k \in \mathbb{K}, \\ 0, & k \notin \mathbb{K}, \end{cases} \end{aligned} \tag{14}$$

where $\mathbb{K} = \{q2^L, q = 0, 1, \cdots, 2P(L)-1\}$. Hence, $Y_{a,k}$ is non-zero for only the $2P(L)$ carriers in $\mathbb{K}$ and thus does not interfere with any of the ACO-OFDM layers.

For the demodulation of the first layer, the received signal $\mathbf{r}$ is fed into a fast Fourier transform (FFT) module to generate its DFT symbol vector, denoted as $\widetilde{\mathbf{X}}^{(1)}$ in Fig. 2 with elements

$$\widetilde{X}_k^{(1)} = \frac{1}{\sqrt{N}} \sum_{n=0}^{N-1} r_n \exp\left(-j\frac{2\pi}{N}nk\right),\ 0 \leq k \leq N-1. \tag{15}$$

This vector is then utilized to estimate the modulated symbols at the first layer as

$$\widehat{X}_k^{(1)} = \arg \max_{X \in \Omega_X^{(1)}} \left\| X - 2\widetilde{X}_k^{(1)} \right\|^2,\ k = 1, 3, \cdots, N/2-1 \tag{16}$$

where $\Omega_X^{(1)}$ denotes the constellation set of symbols at the first layer and the scalar 2 is due to the zero clipping loss [8].

An ACO-OFDM time-domain signal local estimation $\widehat{x}_{c,n}^{(1)}$ can be generated using an IFFT and clipping, as shown in Fig. 2. The signal $\widehat{x}_{c,n}^{(1)}$ is subtracted from the received signal r_n leading to $\widetilde{x}_n^{(2)}$ that is employed to demodulate the symbols at the second layer.

Demodulation of the other ACO-OFDM layers proceeds in a similar fashion where at layer l, QAM symbols are detected to the DFT symbol vector $\widetilde{\mathbf{X}}^{(l)}$ which arises as the FFT of $\widetilde{\mathbf{x}}^{(l)} = \widetilde{\mathbf{x}}^{(l-1)} - \widehat{\mathbf{x}}_c^{(l-1)}$, i.e., the impact of the detected symbols in the previous layers is removed from subsequent layers.

After the L-th ACO-OFDM layer is detected, the clipping noise on the carriers in $\mathbb{K}$ can be removed by computing the local estimation of $\widehat{\mathbf{x}}_c^{(L)}$ and subtracting it from the remaining signal vector $\widetilde{\mathbf{x}}^{(L)}$. More compactly, an estimate of the AVO-OFDM signal $\widehat{\mathbf{y}}_a = \widetilde{\mathbf{x}}^{(L)} - \widehat{\mathbf{x}}_c^{(L)}$.

In order to be able to demodulate the data in the AVO-OFDM signal, the sign information must be extracted from the first layer of ACO-OFDM. Let $\widehat{s}_n$ denote the detected sign information of the AVO-OFDM signal that is transmitted in layer one. Furthermore, let $\widehat{s}_n^r \in \{-1, 1\}$ denote the sign of the $\widehat{y}_{a,n}$ which is extracted for the first $2P(L)$ symbols by

$$\widehat{s}_n^r = \begin{cases} 1, & \widehat{s}_n = 1; \\ -1, & \widehat{s}_n = 0, \end{cases} \tag{17}$$

where $n = 0, \cdots, 2P(L)-1$. As noted in (9), the AVO-OFDM signal is periodic in period $2P(L)$ and thus, $\widehat{s}_n^r$ can be readily extended for all $n = 0, \cdots, N-1$.

The AVO-OFDM time-domain signal can be reconstructed as

$$\widehat{y}_n^r = \widehat{s}_n^r \widehat{y}_{a,n},\ n = 0, 1, 2, \cdots, N-1. \tag{18}$$

After an N-point FFT module, the AVO-OFDM symbols can be detected using

$$\widehat{Y}_k = \arg \max_{Y \in \Omega_Y} \left\| Y - \widehat{Y}_k^r \right\|^2 \tag{19}$$

where Ω_Y denotes the constellation set of AVO-OFDM, $\widehat{Y}_k^r$ denotes the DFT of $\widehat{y}_n^r$ and $k = q2^L$, $q = 1, 2, \cdots, P(L) - 1$.

As shown in (14), the data carried on by AVO-OFDM does not impact any of the data bearing carriers in the ACO-OFDM layers.

III. Signal analysis

In this section, spectral efficiency and PAPR performance of ALACO-OFDM are analyzed and compared to eU-OFDM [6], LACO-OFDM [8] and AAO-OFDM [3].

A. Spectral efficiency

The spectral efficiency of DCO-OFDM with QAM constellation size M, Υ_{DCO}, can be written as

$$\Upsilon_{\text{DCO}} = \frac{1}{2} \log_2 M \text{ bit/s/Hz}. \tag{20}$$

The spectral efficiency of eU-OFDM with L streams, $\Upsilon_{\text{eU}}^{(L)}$, and of LACO-OFDM with L layers, $\Upsilon_{\text{LA}}^{(L)}$, are equal, which can be calculated by [6], [8]

$$\Upsilon_{\text{eU}}^{(L)} = \Upsilon_{\text{LA}}^{(L)} = \frac{1}{2} \log_2 M - \frac{1}{2^{L+1}} \log_2 M \text{ bit/s/Hz}, \tag{21}$$

in which each stream/layer is assumed to use the same constellation size M.

The spectral efficiency of AAO-OFDM, Υ_{AAO}, can be calculated by [3]

$$\Upsilon_{\text{AAO}} = \frac{1}{4}(\log_2 M_1 + \log_2 M_2) - \frac{1}{2} \text{ bit/s/Hz}, \tag{22}$$

in which the constellation size M_1 and M_2 are assumed for AVO-OFDM and ACO-OFDM component parts, respectively. Setting $M_1 = M_2 = M$, Υ_{AAO} can be rewritten as

$$\Upsilon_{\text{AAO}} = \frac{1}{2} \log_2 M - \frac{1}{2} \text{ bit/s/Hz}. \tag{23}$$

In the proposed ALACO-OFDM, for the l-th ($1 \le l \le L$) layer ACO-OFDM, if the constellation size is assumed to be M_l, each symbol conveys $\log_2 M_l$ bits. For the ACO-OFDM layers, notice that there are $P(l) = \frac{N}{2^{l+1}}$ effective complex symbols before Hermitian symmetry for layer l. For AVO-OFDM, the constellation size is assumed to be M_a and there are $P(L) - 1 = \frac{N}{2^{L+1}} - 1$ effective complex symbols before Hermitian symmetry. Notice also that $2P(L) = \frac{N}{2^L}$ sign bits of AVO-OFDM time-domain signals are inserted uniformly into transmitting symbols at the first layer.

Hence, the spectral efficiency of ALACO-OFDM with L layers, denoted by $\Upsilon_{\text{AL}}^{(L)}$, can be calculated by

$$\begin{aligned} \Upsilon_{\text{AL}}^{(L)} = & \\ & \frac{1}{N} \left(\sum_{l=1}^{L} \frac{N}{2^{l+1}} \log_2 M_l + \left(\frac{N}{2^{L+1}} - 1 \right) \log_2 M_a - \frac{N}{2^L} \right) \\ & \approx \sum_{l=1}^{L} \frac{1}{2^{l+1}} \log_2 M_l + \frac{1}{2^{L+1}} \log_2 M_a - \frac{1}{2^L} \text{ bit/s/Hz} \end{aligned} \tag{24}$$

where the approximation holds for large N.

If $M_l = M_a = M$, $\Upsilon_{\text{AL}}^{(L)}$ can be rewritten as

$$\Upsilon_{\text{AL}}^{(L)} = \frac{1}{2} \log_2 M - \frac{1}{2^L} \text{ bit/s/Hz}. \tag{25}$$

Notice that AAO-OFDM is a special case of ALACO-OFDM with $L = 1$ according to (23) and (25).

The spectral efficiency comparison between ALACO-OFDM and DCO-OFDM, eU-OFDM, LACO-OFDM and AAO-OFDM for large N is depicted with different constellation sizes in Fig. 3. It can be seen that Υ_{AAO}, $\Upsilon_{\text{AL}}^{(2)}$, $\Upsilon_{\text{AL}}^{(3)}$, $\Upsilon_{\text{AL}}^{(4)}$ and Υ_{DCO} are parallel, which indicates a constant gap between them. Additionally, notice that ALACO-OFDM is closest to the spectral efficiency of DCO-OFDM. The difference in spectral efficiency between ALACO- and DCO-OFDM decreases with increasing L as $1/2^L$. For example, for $L = 2$ ALACO-OFDM 0.25 bits/s/Hz less than DCO-OFDM, while at $L = 4$ the difference is only 0.0625 bits/s/Hz. For eU-OFDM and LACO-OFDM, the larger the constellation size, the larger the spectral-efficiency gap compared to DCO-OFDM. When $M > 256$, ALACO-OFDM with $L = 2$ achieves larger spectral efficiency than eU-OFDM and LACO-OFDM with $L = 4$. For the same layer number L, the spectral efficiency of ALACO-OFDM is

$$\frac{\log_2 M - 2}{2^{L+1}} \quad \text{bit/s/Hz}$$

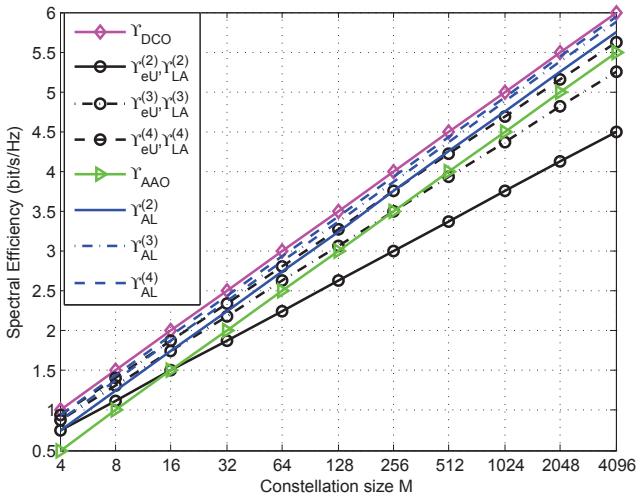

Fig. 3. The spectral efficiency comparison between ALACO-OFDM and its counterparts with different constellation sizes.

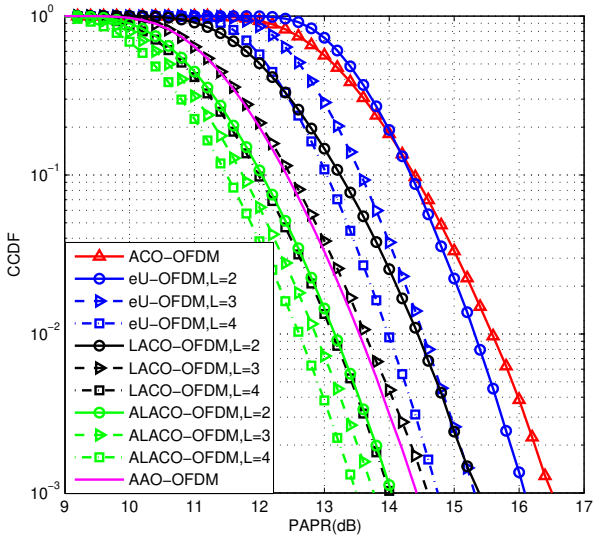

Fig. 4. PAPR comparison between ALACO-OFDM and its counterparts with $N = 1024$ subcarriers.

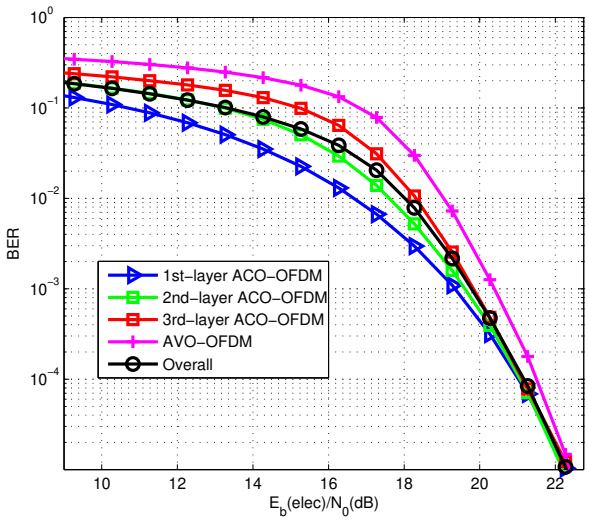

Fig. 5. BER performance of the proposed ALACO-OFDM with $L = 3$.

larger than eU-OFDM and LACO-OFDM.

B. PAPR analysis

In this section, we investigate the PAPR performance of ALACO-OFDM and compare it with ACO-OFDM, LACO-OFDM, eU-OFDM and AAO-OFDM. The PAPR of a discrete time-domain signal z_n can be calculated by [11]

$$\text{PAPR} = \frac{\max\limits_{0\le n\le N-1} z_n^2}{\text{E}\{z_n^2\}} \tag{26}$$

where $\text{E}\{\cdot\}$ denotes the expectation operation.

The complementary cumulative distribution function (CCDF) of PAPR is calculated by

$$\text{CCDF}(\xi) = 1 - \Pr\{\text{PAPR} \le \xi\}, \tag{27}$$

in which $\Pr\{\Pi\}$ denotes the probability of an event Π.

The CCDF of PAPR in ALACO-OFDM with different total layer number L is analyzed and compared to ACO-OFDM, eU-OFDM, LACO-OFDM and AAO-OFDM as shown in Fig. 4 for $N = 1024$. It is evident that ACO-OFDM has the worst PAPR performance. For eU-OFDM, LACO-OFDM and ALACO-OFDM, the PAPR performance becomes better as the total layer number L increases from 2 to 4. This trend was also noticed in earlier work [12]. When CCDF $= 10^{-3}$, the PAPR of ALACO-OFDM with $L = 2$ is about 0.4 dB, 1.3 dB, 2.1 dB and 2.5 dB smaller compared to AAO-OFDM, LACO-OFDM with $L = 2$, eU-OFDM with $L = 2$ and ACO-OFDM, respectively. When CCDF approaches 10^{-3}, the PAPR of ALACO-OFDM with $L = 4$ is about 0.9 dB, 0.5 dB, 1.3 dB and 3.1 dB smaller compared to AAO-OFDM, LACO-OFDM with $L = 4$, eU-OFDM with $L = 4$ and ACO-OFDM, respectively. The analysis and comparison between ALACO-OFDM and its counterparts suggests that ALACO-OFDM may be less sensitive to LED nonlinearity.

IV. Numerical Results

In this section, BER performance of ALACO-OFDM is analyzed and compared to its counterparts in terms of normalized electrical bit energy to noise power ratio $E_b(\text{elec})/N_0$ [6]. A flat channel with AWGN is assumed and the channel gain from an LED to a PD is assumed to be unity [5], [6]. The total number of subcarriers is set to $N = 1024$. As in earlier eU-OFDM [6], LACO-OFDM [8] and AAO-OFDM [3] work, the electrical power of each modulated subcarrier prior to clipping or absolute value is assumed to be equal. In all cases, QAM constellations with Gray labelling are employed.

The BER performance for each layer of ALACO-OFDM is shown in Fig. 5, where $L = 3$ and $M = 16$ is employed. In this case, the spectral efficiency is $\Upsilon_{\text{AL}}^{(3)} = 1.875$ bit/s/Hz following (25). The average BER of each layer ACO-OFDM, AVO-OFDM and the overall performance are presented. When the SNR is small, the BER performance of l-th ($1 \le l \le 3$) layer ACO-OFDM becomes worse as l increases for same $E_b(\text{elec})/N_0$. The bits sent via AVO-OFDM has the probability of error. This is reasonable since symbols in higher layers are distorted not only by AWGN but also the estimation error of lower layers. As the SNR increases, the BER of all layer ACO-OFDM and AVO-OFDM have similar performance because estimation error in lower layers becomes negligible. Given that most VLC channels operate in the high SNR regime [13], the difference in BER performance between layers may be practically insignificant.

The BER performance of ALACO-OFDM is compared to eU-OFDM, LACO-OFDM and AAO-OFDM as shown in Fig. 6 with the same or close spectral efficiency and finite number of layers. For ALACO-OFDM, $M = 256$ with $L = 2$, 3 or 4 is employed, of which has spectral efficiency is $\Upsilon_{\text{AL}}^{(L)} = 3.75$, 3.875 or 3.9375 bit/s/Hz according to (25). For eU-OFDM and LACO-OFDM, combinations of $M = 1024$ with $L = 2$,

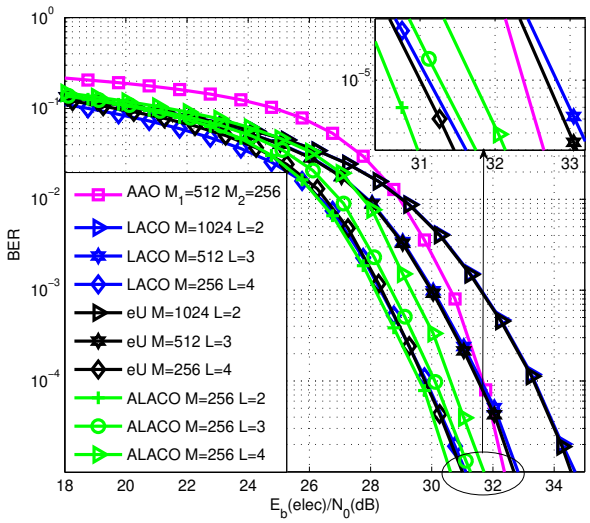

Fig. 6. BER performance comparison between ALACO-OFDM and its counterparts with the same or close spectral efficiency (Set $\Upsilon_{\text{AAO}} = \Upsilon_{\text{eU}}^{(2)} = \Upsilon_{\text{LA}}^{(2)} = \Upsilon_{\text{AL}}^{(2)} = \Upsilon_{\text{eU}}^{(4)} = \Upsilon_{\text{LA}}^{(4)} = 3.75$ bit/s/Hz, $\Upsilon_{\text{eU}}^{(3)} = \Upsilon_{\text{LA}}^{(3)} = \Upsilon_{\text{AL}}^{(4)} = 3.9375$ bit/s/Hz, and $\Upsilon_{\text{AL}}^{(3)} = 3.875$ bit/s/Hz).

$M = 512$ with $L = 3$ and $M = 256$ with $L = 4$ are utilized, of which the spectral efficiency is respectively 3.75, 3.9375 and 3.75 bit/s/Hz based on (21). For AAO-OFDM, $M_1 = 512$ and $M_2 = 1024$ are employed yielding $\Upsilon_{\text{AAO}} = 3.75$ bit/s/Hz from (22). It can be seen that eU-OFDM and LACO-OFDM have the similar BER performance with the same layer number and constellation size, in which the spectral efficiencies of the both schemes are the same.

Figure 6 indicates that ALACO-OFDM with $M = 256$ and $L = 2$ has the best BER performance compared to eU-OFDM with $M = 1024$ and $L = 2$, LACO-OFDM with $M = 1024$ and $L = 2$ and AAO-OFDM with $M_1 = 512$ and $M_2 = 1024$ at the same spectral efficiency of 3.75 bit/s/Hz. When the BER approaches 10^{-5}, it achieves about 3.9, 4.1 and 1.8 dB performance gains over eU-, LACO- and AAO-OFDM, respectively. This is because ALACO-OFDM has the highest spectral efficiency compared to the other three schemes and can employ the smallest constellation size M.

From the spectral efficiency analysis in section III-A, increasing L improves the spectral efficiency of ALACO-OFDM, eU-OFDM and LACO-OFDM. Notice that ALACO-OFDM with $M = 256$ and $L = 2$ has a 0.4 dB gain over eU-OFDM and LACO-OFDM with $M = 256$ and $L = 4$ at BER=10^{-5}. The spectral efficiencies of all schemes noted are the same, however, ALACO-OFDM is able to provide a gain while operating with less complexity and latency (i.e., smaller L). Similarly at a higher spectral efficiency, ALACO-OFDM with $M = 256$ and $L = 4$ achieves a 1.0 dB gain at BER= 10^{-5} compared to eU-OFDM and LACO-OFDM with $M = 512$ and $L = 3$ at the spectral efficiency of 3.9375 bit/s/Hz. These gains are apparent at high SNR, however, at lower SNRs ALACO-OFDM has slightly worse performance due to the sensitivity of the sign bits in the AVO-OFDM layer. Thus, ALACO-OFDM provides higher spectral efficiencies over earlier approaches while retaining the power efficiency of ACO-OFDM schemes with smaller complexity and latency over LACO-OFDM and eU-OFDM.

V. Conclusions

In this paper, ALACO-OFDM is proposed to enhance the spectral efficiency for IM/DD OFDM communications while retaining power efficiency. Signal analysis indicates the spectral efficiency gap between ALACO-OFDM and DCO-OFDM is a constant that can be further reduced by increasing the total layer number L. The spectral efficiency of ALACO-OFDM is $1/2^L$ bit/s/Hz bigger than AAO-OFDM, and $\frac{\log_2 M-2}{2^{L+1}}$ bit/s/Hz bigger compared to eU-OFDM and LACO-OFDM with the same layer number L. In addition, ALACO-OFDM has smaller PAPR compared to eU-OFDM, LACO-OFDM and AAO-OFDM, which suggests better performance on nonlinear LED channels. Monte Carlo simulation of BER performance is analyzed and compared, from which it can be concluded that ALACO-OFDM has the best BER performance with the same spectral efficiency while using a smaller number of layers.

References

[1] L. Hanzo, H. Haas, S. Imre, D. O'Brien, M. Rupp, and L. Gyongyosi, "Wireless myths, realities, and futures: from 3G/4G to optical and quantum wireless," *Proc. IEEE*, vol. 100, no. Centennial Special Issue, pp. 1853–1888, May 2012.

[2] J. M. Kahn and J. R. Barry, "Wireless infrared communications," *IEEE Proc.* vol. 85, no. 2, pp. 265-298, Feb. 1997.

[3] R. Bai, Q. Wang and Z. Wang, "Asymmetrically clipped absolute value optical OFDM for intensity-modulated direct-detection systems," *J. Lightw. Technol.*, vol. 35, no. 17, pp. 3680–3691, Sep. 2017.

[4] J. Armstrong, "OFDM for optical communications," *J. Lightw. Technol.*, vol. 27, no. 3, pp. 189–204, Feb. 2009.

[5] S. D. Dissanayake and J. Armstrong, "Comparison of ACO-OFDM, DCO-OFDM and ADO-OFDM in IM/DD systems," *J. Lightw. Technol.*, vol. 31, no. 7, pp. 1063–1072, Apr. 2013.

[6] D. Tsonev and H. Haas, "Avoiding spectral efficiency loss in unipolar OFDM for optical wireless communication," in *Proc. of the International Conference on Communications* (ICC), Sydney, Australia: IEEE, Jun., 10-14 2014, pp. 3336-3341.

[7] L. Chen, B. Krongold, and J. Evans, "Successive decoding of anti-periodic OFDM signals in IM/DD optical channel," in *Proc. IEEE International Conference on Communications* (ICC), Cape Town, South Africa, 2010, pp.1–6.

[8] Q. Wang, C. Qian, X. Guo, Z. Wang, D. G. Cunningham, and I. H. White, "Layered ACO-OFDM for intensity-modulated direct detection optical wireless transmission," *Opt. Exp.*, vol. 23, no. 9, pp. 12382–12393, May 2015.

[9] M. S. Islim, D. Tsonev, and H. Haas, "On the superposition modulation for OFDM-based optical wireless communication," in *Proc. IEEE Global Conference on Signal and Information Processing* (GlobalSIP), Orlando, FL, 2015, pp. 1022–1026.

[10] Q. Wang, B. Song, B. Corcoran, D. Boland, C. Zhu, L. Zhuang, and A. J. Lowery, "Hardware-efficient signal generation of layered/enhanced ACO-OFDM for short-haul fiber-optic links," *Opt. Exp.*, vol. 25, no. 12, pp. 13359–13371, Jun. 2017.

[11] J. Wang, Y. Xu, X. Ling, R. Zhang, Z. Ding, and C. Zhao, "PAPR analysis for OFDM visible light communication," *Opt. Exp.*, vol. 24, no. 24, pp. 27457–27474, Nov. 2016.

[12] X. Zhang, Q. Wang, R. Zhang, S. Chen and L. Hanzo, "Performance Analysis of Layered ACO-OFDM," *IEEE Access*, vol. 5, pp. 18366–18381, Sep. 2017.

[13] J. Grubor, S. Randel, K.-D. Langer, and J. Walewski, "Broadband information broadcasting using LED-based interior lighting," *J. Lightw. Technol.*, vol. 26, no. 24, pp. 3883–3892, Dec. 2008.